NORSAR Scientific Report No. 2-2004

Semiannual Technical Summary

1 January - 30 June 2004

Frode Ringdal (ed.)

Kjeller, August 2004

6.4 Discriminants for seismic monitoring

6.4.1 Introduction

In this study a number of different discriminants are calculated for a set of seismic events. The data consists of recordings of events presumed to be mining explosions, underwater explosions, other types of explosions, and earthquakes. Recordings from the seismic arrays HFS and ARCES are used, and the events are located at distances up to 700 km from these arrays. Fig. 6.4.1 shows a map where events and seismic stations are marked with different symbols.

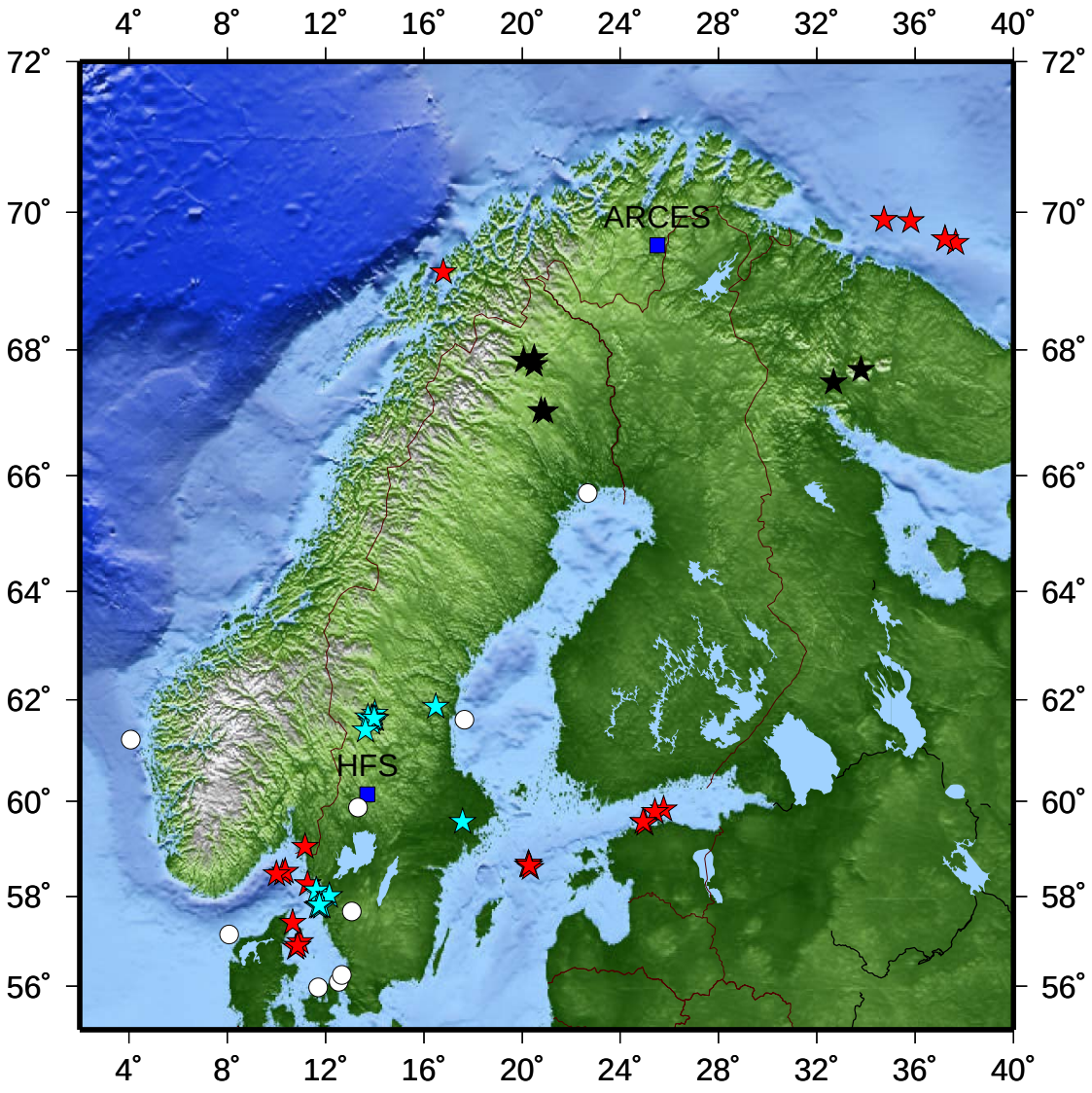

Fig. 6.4.1. Seismic events and array stations used in this study. The stars and circles indicate the presumed types of events, where black stars are mining explosions, red stars are underwater explosions, cyan stars are other types of explosions, and circles are earthquakes. The squares mark the seismic array stations HFS and ARCES.

The main objective is to discriminate recordings with spectral modulation from other recordings. It is known that spectral modulation appears for recordings originating from ripple fired explosions (common in mining, see Hedlin et al., 1998), and underwater explosions. A second objective is to discriminate between other types of seismic events, using classical discriminants.

The discriminants considered here are the following:

- Maximum peak in the cepstrum
- P/S ratio
- Complexity
- Third moment of frequency (TMF)
- Spectral misfit to earthquake (mean square error of the best fit)

It should be stressed that the discriminants most certainly can be optimized by tuning the processing parameters, compensating for the effects of epicentral distance and prefiltering of the data.

6.4.2 The discriminants

The cepstrum definition used here is $C(\tau) = P(\log\{P(f)\})$, where $P(f)$ is the ordinary power spectrum (see Kanasewich, 1981). When estimating the cepstrum, the power spectrum is first estimated with Welch's method. The spectrum calculation uses the first 40 seconds after the first P-phase, and is calculated for $4f_s$ frequency bins, a Hamming window with $3f_s$ samples and 25% overlap (here f_s is the sampling frequency). The power spectrum is also estimated for noise prior to the first P-phase. For the largest possible frequency interval, where the signal to noise ratio is greater than or equal to 3 dB, the cepstrum is calculated, again with Welch's method. The cepstrum estimator used here is not optimized for time-lag resolution, but rather chosen to simplify interpretation of the cepstrum (usually one main peak appears in the estimate). The value of the maximum cepstrum peak is used as a discriminant. A high peak indicates strong modulation in the spectrum.

The *P/S* ratio used is fairly primitive, not taking the distance to the source into account. The energy for the first 2.5 seconds of the first P-phase (in the frequency interval 2 - 12 Hz) and the energy for the first 2.5 seconds of the first S-phase (in the frequency interval 2 - 8 Hz) are used. The ratio of these two energies is the *P/S* discriminant. Explosions are expected to generate relatively strong P-phases as compared with S-phases.

A definition of complexity is given in Dahlman and Israelsson (1977). The basic idea is to compare the energy around the first onset with energies in time intervals later in the coda. Here the two complexity measures S_1 and S_2 are defined as

$$S_1 = I_{0,2}/I_{0,7} \text{ and } S_2 = I_{2,5}/I_{0,7}, \text{ where } I_{a,b} = \int_a^b s^2(t)dt \text{ and } s(t)$$

is the time domain signal with the first onset at $t=0$. Generally earthquakes are believed to produce more complex codas than explosions, which can be detected in these measurements.

One discriminant that measures how dominant the higher frequencies are in relation to the lower frequencies in the spectrum is the third moment of frequency, which is here defined as

$$TMF = \left(\frac{\int_{f_0}^{f_1} f^3 A(f) df}{\int_{f_0}^{f_1} A(f) df} \right)^{1/3}$$

where *A(f)* is the amplitude spectrum of the first P-phase. Here $f_0 = 0$, and $f_1 = 5$ is used, which is equivalent to the definition given in Dahlman and Israealsson (1977). Like the *P/S* ratio the spectrum is not corrected for the distance.

In theory, the displacement close to the source of an earthquake should be the convolution of two boxcar pulses (Lay and Wallace, 1995). This generates a displacement spectrum *A(f)*, which consists basically of a constant level for low frequencies, and above a certain cut-off frequency the spectrum decays proportionally to f^{-k} (i.e. linearly for *log(A(f))* as a function of *log(f)*). Depending on which phase is analyzed k can be 1, 2 or 3 (for a P-phase $k=1$). With correction for the source sensor distance the spectrum is basically just tilted and translated to a lower level (the constant level gets a negative slope, and the linear function above the cut-off frequency gets a steeper slope). A fit to a piecewise linear function (two straight lines intersecting at the cut-off frequency) is therefore performed for *log(A)* as a function of *log(f)*. The mean squared error for this fit is then used as a discriminant, and is called the spectral misfit to earthquake. Therefore a low value should indicate an earthquake, and high value some other type of event. This discriminant can be extended to a vector by including the slopes of the two linear functions, and the cut-off frequency. This has not been done, but doing so might improve the separation between the different events.

6.4.3 Data

The list of analyzed events is given in Table 6.4.1, and are mainly chosen from NORSAR's regional reviewed bulletin. Some events have also been chosen from NORSAR's automatic GBF-bulletin (bulletins at NORSAR are available at *http://www.norsar.no/*). The events are presumed to be one of the following four classes:

- Underwater explosions
- Mining explosions
- Other types of explosions
- Earthquakes

Some of the presumed earthquakes are confirmed as felt close to the epicenters in Denmark and Finland (see *http://www.kms.dk/* and *http://www.seismo.helsinki.fi/bul/*, respectively). However most of the presumed earthquakes have not been confirmed in any other way than by interactive analysis and expert assessments.

The category underwater explosions comprises the Kursk accident in the Barents Sea (Ringdal et al., 2000; Savage and Helmberger, 2001; Schweitzer, 2002), and also one of the following explosions for cleaning up the area. Not too far away from the Kursk events two other explo-

sions are included. These are believed to be the Russian missile tests in February 2004 which were reported in the news. Some other underwater explosions are from the Baltic Sea and from Skagerrak.

Mining explosions in the study are taken from three mining areas: Kiruna (Sweden), Malmberget (Sweden) and the Khibiny Massif on the Kola Peninsula, Russia (mine KH4).

Other types of explosions which are included in the study are an explosion from a road construction outside Stockholm and explosions from ammunition destruction sites in Sweden situated at Mossibränden and Älvdalen. The events in Mossibränden and Älvdalen are confirmed; 8 of these explosions took place on the surface, one took place underground and was decoupled. General information about similar explosions in Mossibränden and Älvdalen are given by Gibbons et al. (2002). Also some unknown explosions near the West Coast of Sweden are included (some of these are possibly underwater explosions).

The seismic arrays which have been used are HFS situated near Hagfors in Sweden, and ARCES situated near Karasjok in northern Norway. The used seismometers at are all vertical component and of type GS-13, at HFS sampled at 80 Hz, and at ARCES sampled at 40 Hz.

For HFS, all sensors are used, covering an aperture of about 1.5 km, whereas only the 8 innermost sensors of the ARCES array are used, covering an aperture of about 600 m. For spectral estimates, the mean of the estimates from individual sensors have been calculated. Similarly, the mean is used for energy estimates of the signals.

Table 6.4.1. Information about the events used. Origin time is given in year, day number and time. In the column 'Array' the array used is specified. Class specifies the type of event (EQ=Earthquake, MX=mining explosion, UWX=underwater explosion, X=other explosion). Countries are abbreviated according to Sweden (Se), Norway (No), Denmark (Dk), Finland (Sf) and Russia (Ru).

Origin time	Lat	Lon	Mag	Array	Class	Comments
2000-225:07.30.41.76	69.573	37.643	3.50	ARC	UWX	Barents Sea, Kursk accident
2001-294:00.31.29.71	57.172	8.082	3.28	HFS	EQ	E. North Sea. Felt in Dk
2001-310:18.05.30.71	55.975	11.705	2.69	HFS	EQ	Sjaelland,Dk. Felt in Dk
2002-164:08.59.25.75	61.410	13.629	1.43	HFS	X	Älvdalen, Se
2002-176:10.04.52.64	61.559	13.879	1.87	HFS	X	Mossibränden, Se
2002-176:14.00.14.00	61.600	13.850	1.77	HFS	X	Mossibränden, Se
2002-251:17.16.28.51	69.628	37.221	2.75	ARC	UWX	Barents Sea, Kursk cleaning up.
2003-004:17.47.58.31	61.868	16.483	2.69	HFS	X	Gävleborg, Se
2003-022:10.41.42.87	58.068	11.715	2.08	HFS	X	Värmland, Se
2003-022:21.05.08.83	58.125	11.617	1.92	HFS	X	Värmland, Se
2003-023:16.13.55.50	58.011	12.166	2.27	HFS	X	Värmland, Se
2003-056:09.09.40.49	57.670	13.071	2.33	HFS	EQ	S.W. Götaland, Se
2003-071:11.01.51.72	56.883	10.792	2.18	HFS	UWX	Jylland, Dk
2003-071:20.15.42.77	57.422	10.670	2.24	HFS	UWX	Jylland, Dk
2003-071:23.28.08.43	56.913	10.865	1.96	HFS	UWX	Jylland, Dk
2003-072:01.19.39.57	56.996	10.980	2.50	HFS	UWX	Jylland, Dk

Origin time	Lat	Lon	Mag	Ar-ray	Class	Comments
2003-133:06.49.36.07	57.777	11.864	2.01	HFS	X	S.W. Götaland, Se
2003-135:08.23.48.88	57.778	11.688	2.36	HFS	X	S.W. Götaland, Se
2003-139:07.18.21.06	57.780	11.742	2.35	HFS	X	S.W. Götaland, Se
2003-144:20.19.07.25	57.812	11.753	2.11	HFS	X	S.W. Götaland, Se
2003-182:07.21.12.32	61.734	14.018	1.78	HFS	X	Mossibränden, Se
2003-182:12.17.02.09	61.656	13.890	1.93	HFS	X	Mossibränden, Se
2003-183:09.47.01.00	61.633	13.918	1.74	HFS	X	Mossibränden, Se
2003-183:14.06.41.13	61.627	14.044	1.88	HFS	X	Mossibränden, Se
2003-184:09.17.01.78	61.662	13.725	1.80	HFS	X	Mossibränden, Se
2003-184:13.31.44.92	61.644	13.989	1.79	HFS	X	Mossibränden, Se
2003-234:03.49.32.38	56.256	12.668	3.07	HFS	EQ	Malmöhus, Se
2003-236:03.42.29.03	61.612	17.649	2.11	HFS	EQ	S. Gulf of Bothnia
2003-245:12.20.58.33	59.875	13.313	2.25	HFS	EQ	Värmland, Se
2003-255:07.23.56.57	59.830	25.759	2.61	HFS	UWX	Gulf of Finland
2003-255:07.44.32.93	59.784	25.420	2.61	HFS	UWX	Gulf of Finland
2003-255:08.44.07.65	59.541	24.995	2.72	HFS	UWX	Gulf of Finland
2003-255:09.16.44.44	59.575	24.931	2.37	HFS	UWX	Gulf of Finland
2003-259:21.37.48.40	58.662	20.246	2.52	HFS	UWX	Baltic Sea
2003-260:00.37.14.53	58.697	20.265	2.28	HFS	UWX	Baltic Sea
2003-260:06.16.24.44	58.607	20.330	2.46	HFS	UWX	Baltic Sea
2003-260:14.47.40.77	58.669	20.286	2.45	HFS	UWX	Baltic Sea
2003-273:14.54.26.00	60.580	15.220	1.28	HFS	X	Gävleborg, Se
2003-273:14.56.50.30	59.054	11.182	2.50	HFS	UWX	Värmland, Se
2003-295:01.55.00.74	65.709	22.679	3.08	HFS ARC	EQ	Bothnian region, Se. Felt in Sf
2003-308:12.48.35.78	67.686	33.790	1.99	ARC	MX	KH4,Kola Peninsula, Ru
2003-338:20.04.18.39	58.490	10.250	2.66	HFS	UWX	Skagerrak
2003-339:12.32.20.14	67.502	32.690	2.50	ARC	MX	KH4,Kola Peninsula, Ru
2004-007:00.19.56.39	67.874	20.501	2.01	ARC	MX	Kiruna, Se
2004-008:00.16.38.20	67.839	20.062	2.13	ARC	MX	Kiruna, Se
2004-013:18.00.48.41	67.051	20.763	1.97	ARC	MX	Malmberget, Se
2004-016:18.12.12.08	67.033	20.925	2.24	ARC	MX	Malmberget, Se
2004-030:00.16.08.19	67.769	20.504	1.95	ARC	MX	Kiruna, Se
2004-034:03.26.17.73	58.524	10.361	2.18	HFS	UWX	Skagerrak
2004-034:03.37.29.05	58.477	10.011	1.67	HFS	UWX	Skagerrak
2004-043:13.04.09.98	58.264	11.265	2.51	HFS	UWX	Skagerrak
2004-048:09.22.49.95	69.820	34.336	1.19	ARC	UWX	Barents Sea, Missile test
2004-048:09.26.34.36	69.942	34.310	1.17	ARC	UWX	Barents Sea, Missile test
2004-054:08.38.30.90	56.111	12.534	2.77	HFS	EQ	Malmöhus, Se. Felt in Dk
2004-058:18.11.59.76	61.107	4.113	3.16	HFS	EQ	N. North Sea
2004-062:14.06.57.03	59.578	17.572	1.96	HFS	X	Road work, Stockholm, Se
2004-074:12.30.50.90	69.155	16.797	2.31	ARC	UWX	Troms, No

Based on the onset times for the first P-phase, waveform segments have been collected, starting 20 seconds before the onset and with a total length of 320 seconds. Some bulletin information such as arrival times for different phases have been used in order to calculate the discriminants, but most of the calculations rely on the waveforms directly.

6.4.4 Results

The performance of the discriminants using the data is presented in Figs 6.4.2-6.4.5. The discriminants for all the events are presented in pairs. Different symbols or colors are used for different types of events.

We see from Fig. 6.4.2 that by using a combination of the cepstral peak and the spectral misfit to an earthquake, the earthquakes are well separated from underwater explosions and mining explosions. The other types of explosions are generally not separated from the earthquake population.

The *P/S* relation seems to perform well when it comes to separating explosions from earthquakes (see Fig. 6.4.3). However, the ratio has only been calculated for events where body-wave S-phases exist in the bulletin.

The third moment of frequency does not separate different classes of events satisfactorily (see Fig. 6.4.4), the earthquakes are also spread out in the feature space. The same holds for the complexity discriminants (Fig. 6.4.5), although these are slightly better. These methods might require tuning and adjustments.

One of the earthquakes seems to stand out from the rest (this is the presumed earthquake in E. North Sea in 2001-294). It has high spectral misfit, a high *P/S* ratio, and a high S_1- complexity, however, it has a normal cepstral peak. This event should probably be considered as an outlier, but because of the quite limited number of events, there is too little data to obtain a reliable assessment of the statistical properties of the discriminants.

Generally the presented discriminants do not separate explosions from earthquakes, but ripple fired explosions and underwater explosions seem to separate from the other types of events reasonably well.

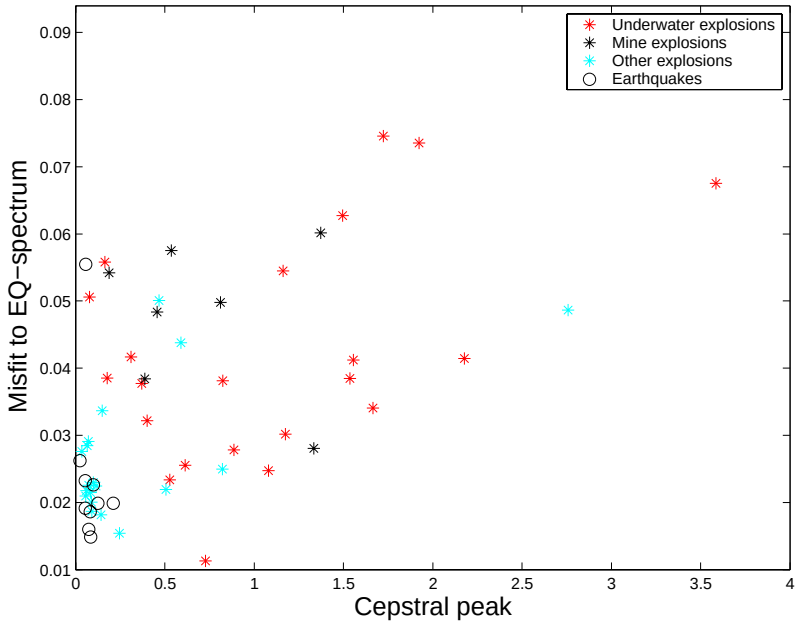

Fig. 6.4.2. Distribution of the maximum cepstral peaks and the spectral misfit to earthquake for the dataset given in Table 6.4.1.

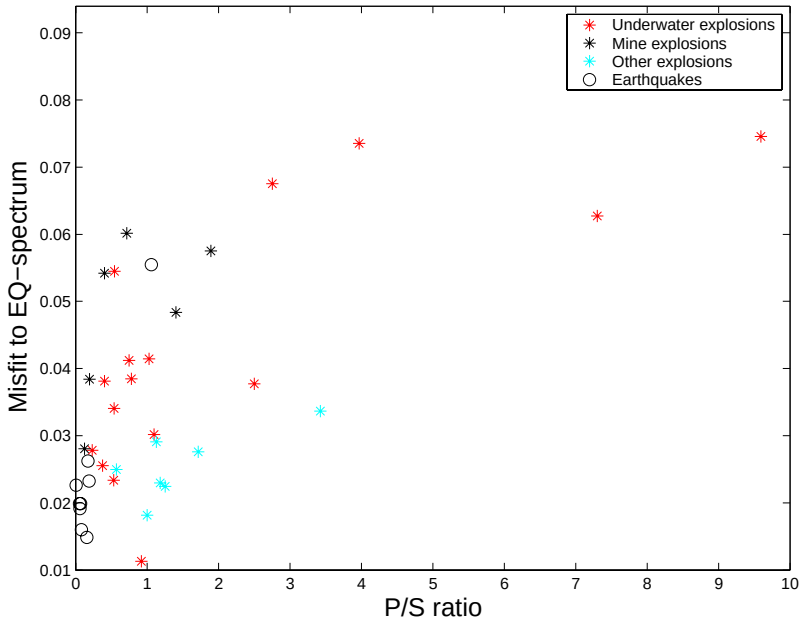

Fig. 6.4.3. Distribution of the P/S ratio and spectral misfit to earthquake for the dataset given in Table 6.4.1. The events where P/S could not be calculated are not represented in the figure.

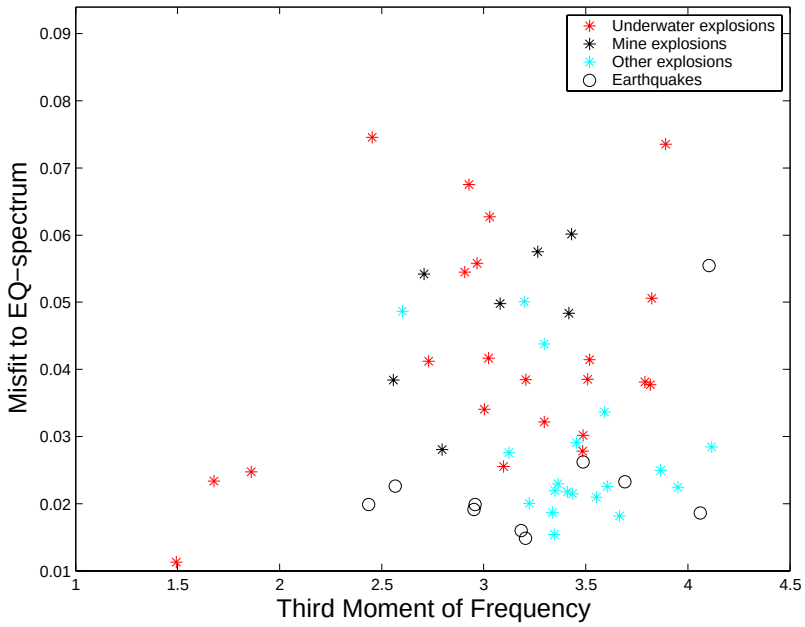

Fig. 6.4.4. Distribution of the TMF and spectral misfit to earthquake for the dataset given in Table 6.4.1.

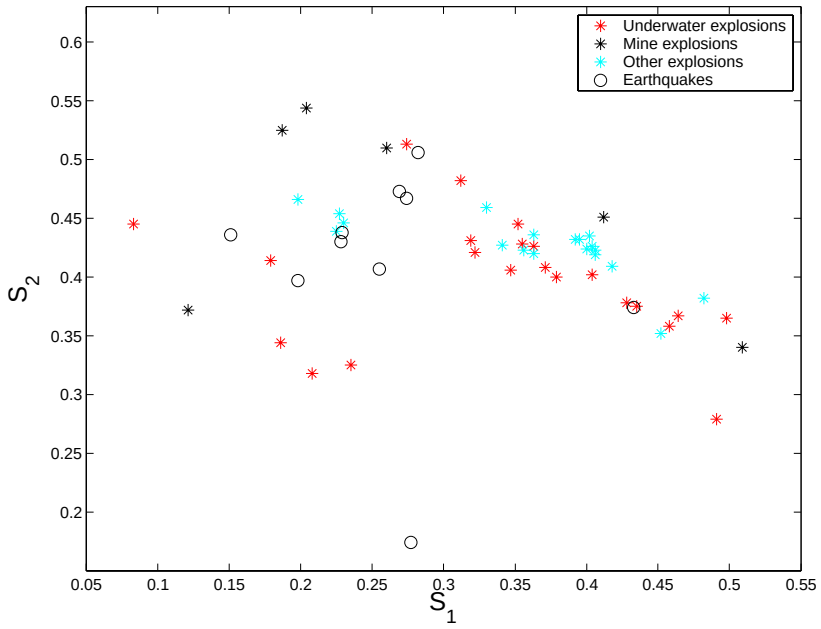

Fig. 6.4.5. Distribution of the two complexity-discriminants for the dataset given in Table 6.4.1.

Four events are studied in more detail, as shown in Fig. 6.4.6 to Fig. 6.4.9. In these figures seismograms are presented, along with the corresponding spectrograms, for 100 seconds of data. Bulletin information, which also specifies the identified phases, is presented in the upper part of the panels. The phases are also marked in the seismograms. Cepstra and spectra of the first P-phases (with spectral fit to earthquake) appear to the right in the panels. Finally the P/S ratios are presented above the seismograms ('NaN'=Not a number (see Fig. 6.4.9), means that P/S could not be calculated, because of missing information about S_n- and S_g-phases).

The four events are the Kursk accident (Fig. 6.4.6), a mining explosion in Sweden (Fig. 6.4.7), an earthquake in Sweden (Fig. 6.4.8), and an ammunition destruction explosion in Sweden (Fig. 6.4.9). The two first show strong spectral modulation, while the two latter do not have this feature. The spectral fit to earthquake is also poor for the first two events, while the last two show better fit. The earthquake has a low P/S value, while the explosions have high values (for the ammunition destruction explosion this value could not be computed).

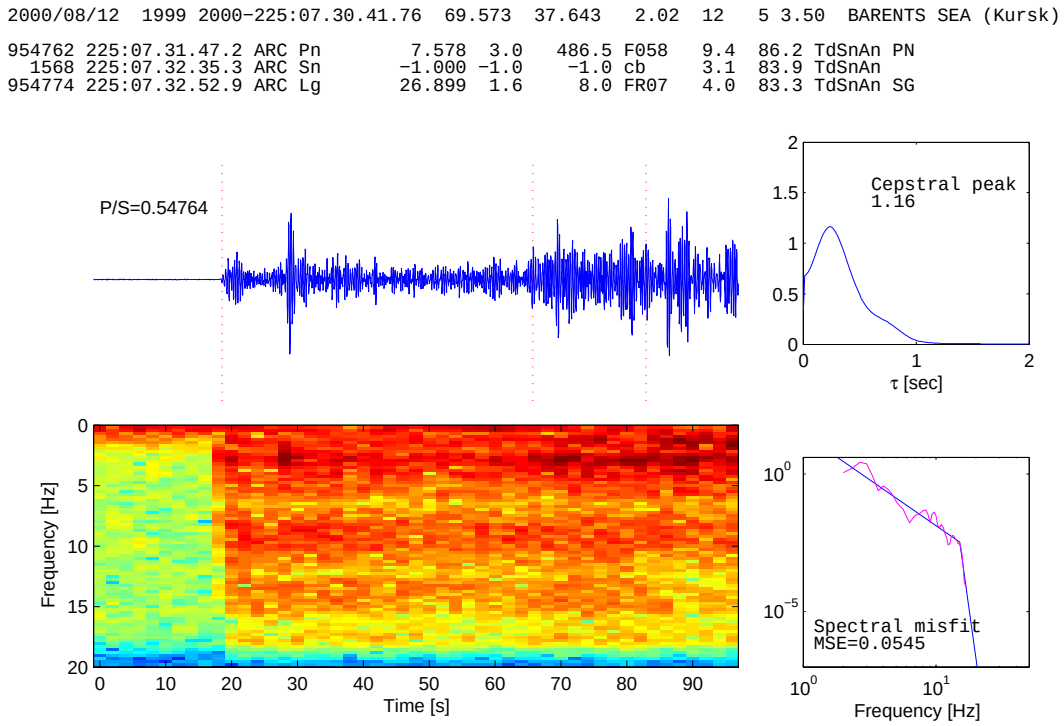

Fig. 6.4.6. Spectrogram, Cepstrum and spectral misfit for the event from the Kursk accident, Barents Sea

```
2004/01/13  5987 2004-013:18.00.48.41  67.051  20.763   0.88   5   2 1.97  CENTRAL NORBOTTEN S

537873 013:18.01.37.5 ARC Pn        1.640  5.5   191.9 FG32   7.9 211.9 TdSnAd PN
537895 013:18.02.15.2 ARC Sn        3.268  5.1     5.8 FT20   5.3 222.4 TdSnAd SG
```

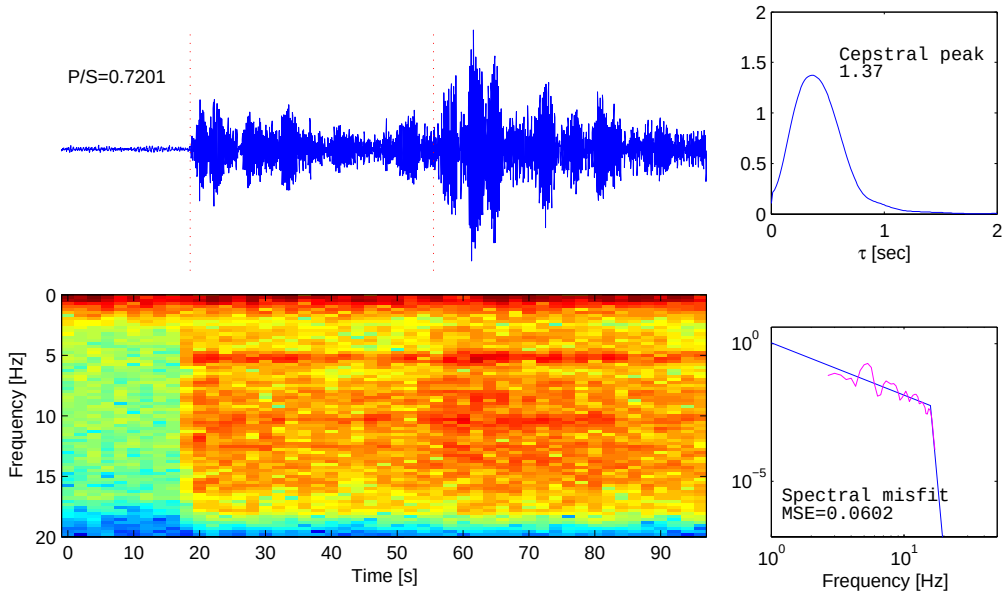

Fig. 6.4.7. Spectrogram, Cepstrum and spectral misfit from a mining explosion in Malmberget, Sweden.

```
2003/02/25  5094 2003-056:09.09.40.49  57.670  13.071   1.24   7   3 2.33  SOUTH-WESTERN GOETA

701138 056:09.10.21.0 HFS Pn        0.679  6.7    16.4 HB17   7.3 182.8 TdSnAd PG
701146 056:09.10.52.1 HFS Sn        3.909  7.5    14.3 HH03   4.5 191.5 TdSnAd SN
701147 056:09.10.59.3 HFS Lg        9.512  3.8    31.9 HF21   3.8 190.0 TdSnAd SG
```

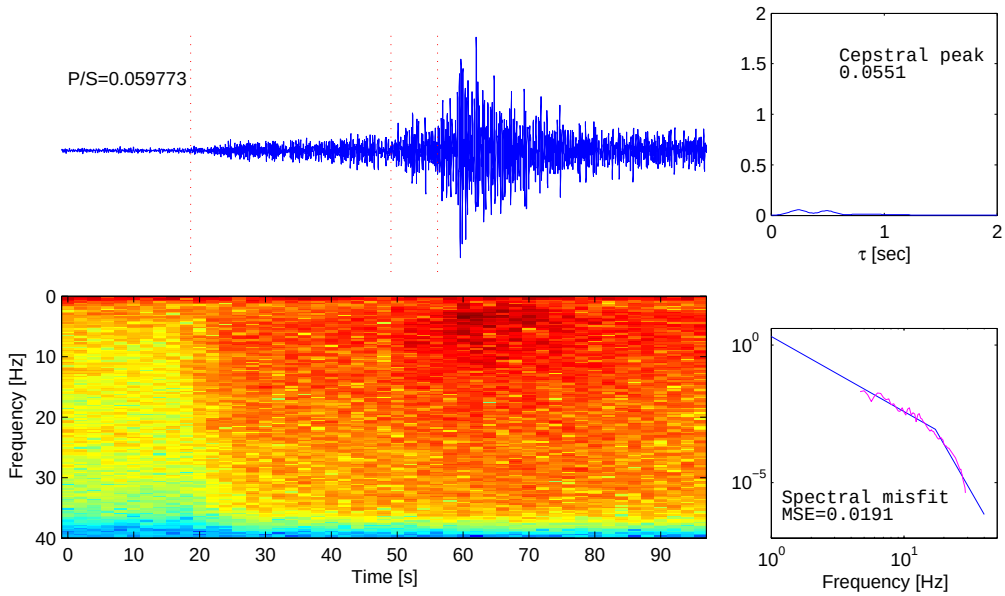

Fig. 6.4.8. Spectrogram, Cepstrum and spectral misfit from an earthquake in south west Sweden.

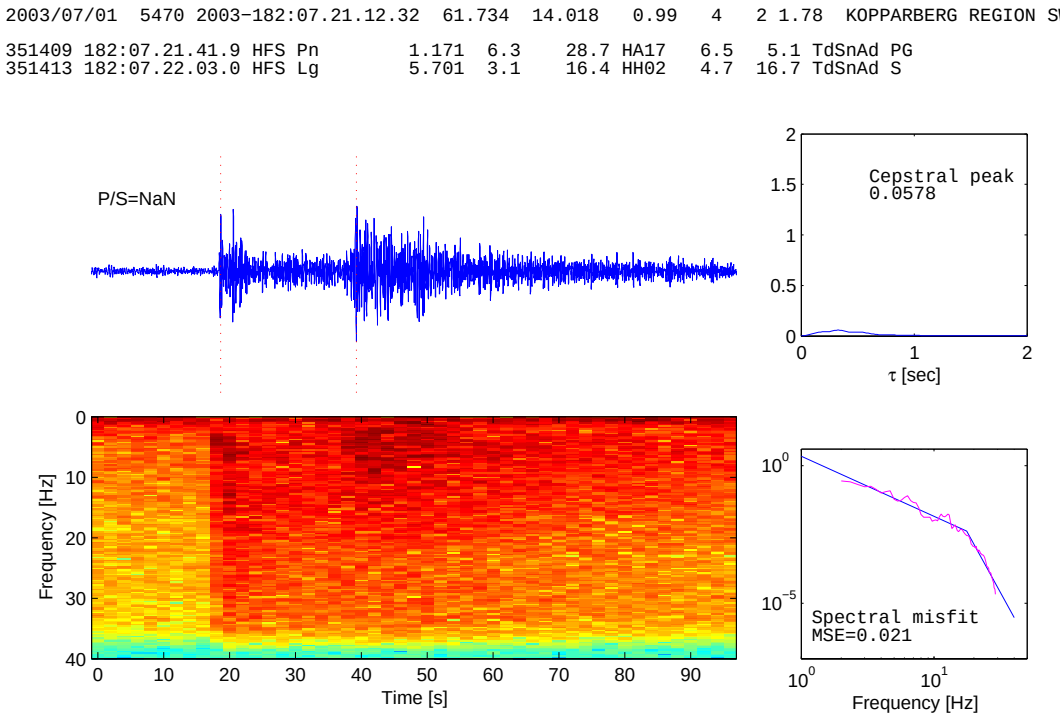

Fig. 6.4.9. Spectrogram, Cepstrum and spectral misfit from an ammunition destruction explosion in Mossibränden, Sweden.

6.4.5 Discussion

One of the earthquakes is definitely an outlier in terms misfit to an earthquake spectrum and also for the P/S ratio. This is the 2001-294 event which was reported felt in Denmark. This earthquake had, however, a cepstral peak that was consistent with the other earthquakes. Since this is the only earthquake that does not fall within the earthquake clusters of Figures 2 and 3, it would be interesting to study it further in greater detail. We would also like to further investigate the algorithm for calculation of the spectral misfit to an earthquake spectrum, in particular for cases when the cut-off frequency is close to the Nyquist frequency of the data (e.g., see Fig. 6.4.7).

The sampling rate of the data is quite high (80 Hz for HFS, and there exists a 100 Hz three-component instrument at ARCES), so that it is possible to consider significantly higher frequencies for the P/S ratio and third moment of frequency. This is particularly interesting since frequencies as high as 40-50 Hz have not previously been studied in detail for discrimination of regional events.

The database used in this study comprises 57 seismic events which is a relatively small database taking into account the large size of the region. A natural extension to this study will be to expand the database considerably. In this connection we note that there are many regions for which comprehensive ground-truth data is available. In particular, this applies to the mining regions of the Kola Peninsula, but such data are also being accumulated for mines in Sweden and Finland. The earthquake population can likewise be expanded considerably, and, in particular the Finnish regional bulletin could be useful for this purpose. Many additional events can

be classified with high certainty as underwater explosions, especially in the Baltic Sea and offshore Norway. Although ground-truth information is not available for these presumed explosions, they can nevertheless be valuable data in these type of studies.

By expanding the dataset as outlined, it would be possible to regionalize the study of the discriminants. It would be of particular interest to study subsets of approximately co-located events of various source types. This would be expected to contribute to a reduction in the scatter for the discriminants, and would thereby enhance their effectiveness in practical operation. A larger database would also make it possible to assess the statistical properties of the discriminants.

Finally, the methods described in this paper lend themselves to automatic or semi-automatic computation on a routine basis, and a script has been developed to facilitate such regular analysis.

Acknowledgements

The 2-month research term of Dan Öberg at NORSAR in 2004 was funded through the EC programme Access to Research Infrastructure (Contract HPRI-CT-2002-00189).

Dan Öberg, FOI, Department of Naval Sensor Systems, Stockholm, Sweden
Tormod Kværna
Frode Ringdal

References

Dahlman, O. and H. Israelsson (1977). Monitoring underground nuclear explosions, Elsevier, Amsterdam.

E.R. Kanasewich (1981). Time sequence analysis in geophysics, 3rd ed., University of Alberta Press, Edmonton.

Gibbons, S., C Lindholm, T. Kværna and F. Ringdal (2002). Analysis of cavity-decoupled chemical explosions. In: NORSAR Semiannual Tech. Summ. 1 January - 30 June 2002, NORSAR Sci. Rep. No. 2-2002, Kjeller, Norway, pp. 78-89

Hedlin M (1998). A global test of a time-frequency small-event discriminant, Bull. Seism. Soc Am. 88, pp. 973-988, August 1998.

Lay, T. and T.C. Wallace (1995). Modern global seismology, Academic Press, San Diego.

Ringdal, F., T. Kværna and B. Paulsen (2000). Seismic events in the Barents Sea at and near the site of the Kursk submarine accident on 12 August 2000. In: NORSAR Semiannual Tech. Summ. 1 April - 30 September 2000, NORSAR Sci. Rep. No. 1-2000/2001, Kjeller, Norway, pp. 77-88

Savage, B. and D.V. Helmberger (2001). Kursk Explosion, Bull. Seism. Soc Am., 91, pp. 753-759.

Schweitzer, J. (2002). Some results derived from the seismic signals of the accident of the Russian submarine Kursk. In: NORSAR Semiannual Tech. Summ. 1 July - 31 December 2001, NORSAR Sci. Rep. No. 1-2002, Kjeller, Norway, pp. 115-121.

6.5 Comparison of the Love-Rayleigh discrepancy in central Europe (GRSN) and southern Scandinavia (NORSAR)

6.5.1 Introduction

The lower crust and mantle are known to be laterally heterogeneous. Furthermore, they are supposed to be anisotropic. However, anisotropy in the upper mantle and the lower crust is a matter of debate, in particular in continental regions and in subduction zones. This question might be investigated by shear-wave splitting studies, but the depth resolution of this method is limited. Investigation of anisotropy by inversion of surface wave observations shows the advantage of a good resolution in depth.

Love-Rayleigh discrepancy denotes the observation that dispersion curves of fundamental Love and Rayleigh modes cannot be explained by the same isotropic one-dimensional model (McEvilly, 1964). It was repeatedly detected in oceanic regions, e.g. in the Pacific (Ekström and Dziewonski, 1998), while for continental regions the amount of the Love-Rayleigh discrepancy was discussed controversially (e.g., Montagner and Tanimoto, 1991). The Love-Rayleigh discrepancy might be explained by radial anisotropy, that means by different velocities for the horizontally polarized SH- and the vertically polarized SV-wave velocities. The fundamental Rayleigh mode is mainly sensitive to the velocity of transversal particle motion in vertical direction, as SV, whereas Love waves are sensitive for velocities in horizontal direction as SH. However, similar effects might be caused by thin isotropic layers of alternating high and low velocities, or by the different influence of lateral heterogeneity or higher modes on the measurements of the phase velocities of Love and Rayleigh waves (Levshin and Ratnikova, 1984; Maupin, 2002). Azimuthal variations in the Love-Rayleigh discrepancy point to azimuthal anisotropy (Maupin, 1985).

Here, we present examples of the investigation of the Love-Rayleigh discrepancy in two tectonically different continental regions: for the Phanerozoic asthenosphere and lithosphere in central Europe and at the border of the Precambrian Baltic Shield.

6.5.2 Method and Measurements

Dispersion curves of the fundamental modes were measured by a two-station method (Meier et al., 2004). One event is recorded at two stations. The cross correlation of the seismograms leads to phase differences and with the known distance between the stations the phase velocities can be calculated. This procedure is repeated for many events. Then, the inversion of averaged phase velocity curves of fundamental surface wave modes yields one-dimensional models of the *S*-wave velocity structure. These are interpreted as a average models describing the structure beneath the paths.

6.5.3 GRSN

Phase velocities of the fundamental Love and Rayleigh modes were determined for two paths between stations of the German Regional Seismic Network (GRSN). This network consists of 16 permanent broadband stations (STS-2) and was installed in the early 1990s. Here, dispersion curves for the two paths BUG-WET and BFO-CLZ were measured (Fig. 6.5.1). The angle between the two paths is about 90 degrees. The lengths of the paths are 473 and 417 km, respectively. For a minimum event magnitude Ms 5.0 and the given geometry and 36 and 72